



**HAL**  
open science

## Structural and microstructural analysis of bifunctional TiO<sub>2</sub>/Al-Zr thin film deposited by hybrid process

Caroline Villardi de Oliveira, Sylvie Migot, Akram Alhussein, Carmen Jiménez, Frédéric Schuster, Jaafar Ghanbaja, Frédéric Sanchette

### ► To cite this version:

Caroline Villardi de Oliveira, Sylvie Migot, Akram Alhussein, Carmen Jiménez, Frédéric Schuster, et al.. Structural and microstructural analysis of bifunctional TiO<sub>2</sub>/Al-Zr thin film deposited by hybrid process. *Thin Solid Films*, 2020, 709, pp.138255. 10.1016/j.tsf.2020.138255 . hal-02927624

**HAL Id: hal-02927624**

**<https://utt.hal.science/hal-02927624>**

Submitted on 22 Aug 2022

**HAL** is a multi-disciplinary open access archive for the deposit and dissemination of scientific research documents, whether they are published or not. The documents may come from teaching and research institutions in France or abroad, or from public or private research centers.

L'archive ouverte pluridisciplinaire **HAL**, est destinée au dépôt et à la diffusion de documents scientifiques de niveau recherche, publiés ou non, émanant des établissements d'enseignement et de recherche français ou étrangers, des laboratoires publics ou privés.



Distributed under a Creative Commons Attribution - NonCommercial 4.0 International License

## **Structural and microstructural analysis of bifunctional TiO<sub>2</sub>/Al-Zr Thin Film deposited by hybrid process.**

Caroline Villardi de Oliveira<sup>1, 2</sup>, Sylvie Migot<sup>3</sup>, Akram Alhussein<sup>1, 2</sup>, Carmen Jiménez<sup>4</sup>, Frédéric Schuster<sup>2, 5</sup>, Jaafar Ghanbaja<sup>3</sup> and Frédéric Sanchette<sup>1, 2</sup>

<sup>1</sup>ICD-LASMIS, Université de Technologie de Troyes CNRS, Antenne de Nogent, Pôle Technologique de Sud Champagne, 52800 Nogent, France

<sup>2</sup>NICCI, LRC CEA-ICD LASMIS, UTT, Antenne de Nogent, Pôle Technologique de Sud Champagne, 52800 Nogent, France

<sup>3</sup>Institut Jean Lamour (UMR CNRS 7198), Université de Lorraine, 54000 Nancy, France

<sup>4</sup>Univ. Grenoble Alpes, CNRS, Grenoble INP, LMGP, 38000 Grenoble, France

<sup>5</sup>CEA, PTCMP, Centre de Saclay, 91191 Gif-sur-Yvette, France

### **Abstract**

An Al-Zr (4 at.% Zr) film is deposited on High Speed Steel substrates by pulsed Direct Current magnetron sputtering in order to provide sacrificial corrosion resistance of steel. A TiO<sub>2</sub> layer is synthesized on the top by aerosol-assisted metal-organic chemical Vapour Deposition (AA-MOCVD) in order to insure anti-biofouling behaviour. TiO<sub>2</sub> coating has a typical CVD microstructure and the film is anatase single phased. The as-deposited Al-Zr film is an extended supersaturated solid solution Al(Zr) of Zr in Al. The AA-MOCVD process is performed at 773 K for 40 minutes. This annealing leads to a fine precipitation of highly coherent metastable Al<sub>3</sub>Zr(L1<sub>2</sub>) phase in the Al(Zr) matrix. Larger precipitates with a needle like morphology, which crystallize in the equilibrium tetragonal Al<sub>3</sub>Zr(D0<sub>23</sub>) phase are also observed. Transmission electron microscopy analysis clearly shows the cube on cube orientation between Al<sub>3</sub>Zr(L1<sub>2</sub>) phase and Al(Zr) matrix. As the cubic Al<sub>3</sub>Zr(L1<sub>2</sub>) metastable phase is beneficial for the mechanical properties of bulk aluminium based alloys, this result opens the investigation field on Al-Zr coatings, which can provide sacrificial protection of steels.

Keywords: Aluminum-zirconium; Titanium dioxide; Thin film; Magnetron sputtering; aerosol-assisted chemical vapor deposition, Structure.

### **1. Introduction**

TiO<sub>2</sub> is a wide band-gap semiconductor with high chemical stability, non-toxicity, and high photoelectric conversion productivity. In recent years, titanium dioxide (TiO<sub>2</sub>) has been extensively investigated for its remarkable UV-photocatalytic and self-cleaning properties, which can, for example, promote the decomposition of present organics into

harmless products under UV light irradiation. This material, with enhanced photocatalytic performances, has been associated with an anti-corrosion Al-Zr film in a previous study [1].

Al-TM (TM= Transition Metal) coatings have been widely studied as potential candidates for sacrificial protection of steels in corrosive media [2-4]. TM is added as alloying element because it has low solid solubility and low diffusivity in aluminium. Very high cooling rates, associated with the condensation of metallic vapour, involved in out of equilibrium Physical Vapour Deposition processes, lead to thermally stable extended solid solutions in Al-TM alloys. In a narrow composition range, an amorphous single phased film can be obtained in these binary alloy films [5]. Concerning bulk Al alloys, it is well known that the addition of elements as Ti, Zr or Hf in aluminium is of great interest for high temperature properties [6, 7]. Many studies report precipitation behaviours in bulk aluminium based alloys. The addition of Zr in Al can favour precipitation of the metastable  $\text{Al}_3\text{Zr}$  with  $L1_2$  structure (FCC) [8]. This (nano) precipitation seems to be very interesting because it provides a precipitation hardening, up to 400h at 650 K for Al-Zr (at.% Zr <0.1) alloys [8]. The ordered  $\text{Al}_3\text{Zr}(L1_2)$  phase has a very low misfit with the Al matrix. This is associated with very low elastic strain interactions [9] that are expected to take place. Among the Al-Zr binary alloy films, Al-Zr (4 at.% Zr) is a good compromise between intrinsic electrochemical behaviours, sacrificial character on steels and hardness [1].

The present work aims to investigate the structural and microstructural properties of the  $\text{TiO}_2/\text{Al-Zr}$  (4 at.% Zr) bilayer film, which has good functional properties. Al-Zr (4 at.% Zr) is deposited on steel by DC magnetron sputtering and  $\text{TiO}_2$  is deposited on Al-Zr using the atmospheric AA-MOCVD method at 773 K for 40 minutes. The effects of this second process on the evolution of Al-Zr structure and microstructure are highlighted.

## 2. Experimental details

### 2.1. Deposition procedure of Al-Zr

The coating was deposited on High Speed Steel substrates, which were rinsed with ethanol and then dried in hot air before ion cleaning and film deposition. The sputtering chamber, illustrated in Fig. 1(a), was pumped down via a mechanical pump and a turbo-molecular pump allowing a base vacuum of  $5.10^{-4}$  Pa. The Al-Zr thin film was deposited by DC magnetron co-sputtering of two pure metallic targets (99.99% purity, 200 mm in

diameter, 6 mm thick), at floating temperature, without bias, in pure argon. Deposition was carried out for 150 minutes resulting in a film thickness of 3  $\mu\text{m}$ . The sample-holder rotation speed was set at 10 rpm in order to obtain a homogeneous film in thickness and composition, which was confirmed by X map analyses. The target to sample distance was fixed at 10 cm. The substrates were sputter-cleaned for 30 min using  $\text{Ar}^+$  ions to remove contamination layers and to improve film adhesion. During this stage, the bias voltage (Radio Frequency mode, 13.56 MHz), argon flow rate and working pressure were kept constant at 200 W, 50 sccm and 0.33 Pa, respectively. The working pressure was kept at 0.33 Pa with a constant argon flow rate of 50 sccm. The film containing 4 at.% Zr was obtained by applying electrical currents to the Al and Zr targets of 2 A (515 W) and 0.22 A (39 W), respectively.

### *2.2 Deposition procedure of $\text{TiO}_2$*

$\text{TiO}_2$  top layer deposition on Si substrates or on the Al-Zr interlayer was performed by AA-MOCVD (Aerosol-Assisted MetalOrganic Chemical Vapour Deposition) using a custom-designed and homemade reactor (Fig. 1(b)) working at atmospheric pressure. Deposition parameters are given in [1, 10]. Titanium (IV) oxide bisacetylacetonate ( $\text{C}_{10}\text{H}_{14}\text{O}_5\text{Ti}$ , Strem Chemicals) was used as a precursor and ethanol as a solvent. The working temperature was 773 K for a deposition time of 40 minutes.

### *2.3. Characterizations*

The chemical composition of the deposited film was obtained in a FEI Quanta 250 field-emission scanning electron microscope (FESEM), by Energy Dispersive X-ray Spectroscopy (EDS) and quantified by Quantax Esprit software. For each sample, the measurement was carried out on multiple zones of the sample showing significant homogeneity. The elements spectra were acquired from SEM images applying a high accelerating voltage of 10 kV and a pressure vacuum of  $10^{-4}$  Pa considering: 60 kcps count mode, 40 keV acquisition range and 2 kcps initial counting rate.

The structure was investigated by X-ray diffraction (XRD) in  $\theta/2\theta$  mode by means of a Bruker AXS D8-Advance diffractometer with monochromatic  $\text{CuK}\alpha 1$  radiation ( $\lambda = 0.15406$  nm) and by Transmission Electron Microscopy in a JEM - ARM 200F Cold FEG TEM/STEM operating at 200 kV and equipped with a spherical aberration (Cs) probe and image correctors (point resolution 0.12 nm in TEM mode and 0.078 nm in STEM

mode). Cross-section TEM samples of films were prepared using a Focused Ion Beam (FIB)- scanning electron microscope (SEM) dual beam system (FEI Helios 600). The TEM samples were prepared by means of a FIB/SEM FEI Helios NanoLab 600i equipped with platinum Gas Injection System. FIB column uses a gallium liquid metal ion source operating up to 30 kV of accelerating voltage. For deposition, commercial FEI MeCpPtMe<sub>3</sub> precursor was used.

### 3. Results and discussion

X-ray diffraction patterns of as-deposited Al-Zr (4 at.% Zr) coating and annealed for 40 minutes in air at a temperature of about 773 K are shown in **Fig. 2**. This annealing treatment has been performed to simulate and investigate eventual structure evolution of Al-Zr coating during the AA-MOCVD process. The as-deposited Al-Zr film seems to be an extended supersaturated solid solution Al(Zr) of zirconium in aluminium. No significant change is detected after annealing except a small peak/shoulder observed at the smaller angles near the (111)<sub>Al(Zr)</sub> reflection. This peak / shoulder can correspond either to the (111) reflection of the cubic Al<sub>3</sub>Zr(L1<sub>2</sub>) ordered phase [11] or to the diffraction of the (114) planes of the Al<sub>3</sub>Zr(DO<sub>23</sub>) tetragonal phase [12]. So, from XRD analysis, the structure and microstructure of the Al-Zr layer seem to be near stable after annealing at 773 K for 40 minutes.

Before the AA-MOCVD process step, the Al-Zr alloy has a columnar microstructure (**Fig. 3**). EDS elemental distribution maps (not shown) have shown that zirconium is homogeneously distributed throughout the layer. The columns are approximately 450 nm wide and the growth is not systematically from the interface to the surface of the film. This coating is clearly single-phased; it is an extended supersaturated solid solution Al(Zr) of zirconium in aluminium, which is consistent with XRD analysis. This solid solution grows without preferential orientation, which is not surprising for an aluminium-based coating deposited without bias at low temperature.

TiO<sub>2</sub> deposited by AA-MOCVD in our conditions grows in the anatase form in the range 673 – 823 K (Fig. 4), which is confirmed by TEM analysis (**Fig 5**). The microstructure is typical of CVD film growth. The interface between Al-Zr and TiO<sub>2</sub> is very thin, conform and without voids.

After the AA-MOCVD process step at a substrate temperature of 773 K for 40 minutes, the Al-Zr (4 at.% Zr) film has a different microstructure (**Fig. 6**). Indeed, dark

precipitates appear clearly in the Bright Field Scanning Transmission Electron Microscopy (STEM, **Fig. 6a**). Scanning-mode transmission electron microscopy coupled to a High-Angle Annular Dark-Field detector (STEM-HAADF), due to the dependence of signal strength with Z, increases the contrast between phases with different atomic numbers; thus, **Fig. 6b** confirms that these precipitates are richer in zirconium than the matrix. These precipitates have clearly two morphologies; needle and spherical. The spherical ones seem to crystallize mainly at the grain boundaries (**Fig. 6**). EDS analyses have shown that the measured zirconium content of these precipitates is in the range 15 to 17.5 at. %.

The compound with the highest aluminium content in the phase diagram is  $\text{Al}_3\text{Zr}$ . Its stable structure, which is of type  $\text{DO}_{23}$ , has a parameter  $a = 4.001 \text{ \AA}$  [13] to be compared with  $a = 4.032 \text{ \AA}$  for Al and a ratio of tetragonality  $c/a = 4.31$ . The  $\text{Al}_3\text{Zr}$  compound also has an ordered metastable structure based on FCC cell but which has the symmetries of a simple cubic; the  $\text{L}_{12}$  type structure (**Fig 7**). The parameter of this phase is very close to that of aluminium,  $a = 4.093 \text{ \AA}$ . Because of the  $\text{Al}_3\text{Zr}(\text{DO}_{23})$   $c/a$  ratio, significantly higher than 4, such an  $\text{Al}_3\text{Zr}$  coherent precipitate with the aluminium matrix will therefore be subjected to high elastic stresses. This makes it unlikely to precipitate this structure in the Al-Zr (4 at.% Zr) film. Moreover, C. Zhang et al. [14] performed first-principles density functional theory calculations. They show that the lattice misfit of Al/ $\text{Al}_3\text{Zr}(\text{L}_{12})$  is small (less than 1,65%) and, concerning the Al/ $\text{Al}_3\text{Zr}(\text{L}_{12})$  interface, the cube on cube orientation with  $(001)\text{Al} // (001)\text{Al}_3\text{Zr}(\text{L}_{12})$  always yield the lowest formation energy. Thus, precipitation of highly coherent  $\text{Al}_3\text{Zr}(\text{L}_{12})$  is expected.

**Fig. 8** shows the bright field images and selected area electron diffraction (SAED) patterns corresponding to the  $[110]$  zone axis. This figure highlights fine spherical precipitates, which have the  $\text{Al}_3\text{Zr}(\text{L}_{12})$  ordered structure. **Fig. 9** also clearly confirms that  $\text{L}_{12}$  type ordered  $\text{Al}_3\text{Zr}$  precipitates are in fine coherency with the Al(Zr) solid solution matrix in cube on cube relationship with  $[100]\text{Al}(\text{Zr}) // [100]\text{Al}_3\text{Zr}(\text{L}_{12})$ ;  $[010]\text{Al}(\text{Zr}) // [010]\text{Al}_3\text{Zr}(\text{L}_{12})$  and  $[001]\text{Al}(\text{Zr}) // [001]\text{Al}_3\text{Zr}(\text{L}_{12})$ . The image obtained by high resolution STEM-HAADF (**Fig. 10**) shows the coherent interfaces, with adaptation of the parameter between the supersaturated solid solution matrix of Zr in Al, and the  $\text{Al}_3\text{Zr}(\text{L}_{12})$  precipitates with higher zirconium content. There is a very small difference in the parameter between the FCC aluminium matrix and the FCC  $\text{L}_{12}$ -type  $\text{Al}_3\text{Zr}$  compound; and since the mismatch is slight, the  $\text{L}_{12}$ -type compound forms

coherent precipitates.

Precipitation of this metastable phase has already been observed in conventional alloys after annealing at temperatures below 773 K [15-17] while annealing at higher temperatures can lead to the precipitation of the stable phase [6, 7]. These precipitates have either a spherical or needle shape. In the Al-Zr (4 at.% Zr) annealed at 773 K for 40 minutes, the needle like morphology precipitates have the stable  $\text{Al}_3\text{Zr}(\text{DO}_{23})$  tetragonal structure (Fig. 11). The Al(Zr) solid solution is highly saturated because of the direct vapour to solid transformation during film growth. This saturation level could explain the kinetic of precipitation of the stable  $\text{Al}_3\text{Zr}(\text{DO}_{23})$  phase at this relatively low temperature for a short time (40 minutes). This result is consistent with that of V. C. Gudla et al. [18] on nanolayered Al-Zr films annealed in-situ in the TEM.

#### 4. Conclusion

A bifunctional  $\text{TiO}_2/\text{Al-Zr}$  Thin Film was deposited by hybrid process; Al-Zr (4 at.% Zr) film was deposited by DC magnetron co-sputtering from two pure metallic targets and  $\text{TiO}_2$  was deposited on the top by AA-MOCVD at atmospheric pressure and 773 K for 40 minutes. It has been shown in a previous work that Al-Zr is a good candidate for corrosion protection of steel substrate and  $\text{TiO}_2$  has good photocatalytic behaviour.

Al-Zr as-deposited film grows with the FCC structure of Al(Zr) solid solution of Zr in Al. The microstructure is columnar, which is typical of coatings obtained by magnetron sputtering.  $\text{TiO}_2$  film grows with the anatase structure and its microstructure is typical of coatings obtained by CVD.

After annealing, the Al-Zr (4 at.% Zr) film, which was initially an extended supersaturated solid solution Al(Zr) of Zr in Al, is a mixture of three phases; the Al(Zr) matrix; spherical precipitates, which have the  $\text{Al}_3\text{Zr}(\text{L}_{12})$  metastable ordered structure and needle like precipitates, which have the stable  $\text{Al}_3\text{Zr}(\text{DO}_{23})$  tetragonal structure. Concerning spherical precipitates, small ones are observed inside the Al(Zr) grains and larger ones are observed at the Al(Zr) grains boundaries. These spherical precipitates are in fine coherency with the Al(Zr) solid solution.

**Funding:** This research was funded by GIP52 (Groupement d'Intérêt Public) Haute-Marne and CEA (Commissariat à l'Énergie Atomique et aux Énergies Alternatives).

## References

- [1] C. Villardi de Oliveira, A. Alhussein, J. Creus, F. Schuster, M. Schlegel, Zhili Dong, C.N Jiménez, F. Sanchette, Bifunctional TiO<sub>2</sub>/AlZr Thin Films on Steel Substrate Combining Corrosion Resistance and Photocatalytic Properties, *Coatings* 9 (2019) 564; doi:10.3390/coatings9090564
- [2] F. Sanchette, Tran-Huu-Loi, C. Frantz, Deposition of metastable aluminium-chromium alloys by r.f. magnetron sputtering from mixed-powder targets, *Surface and Coatings Technology* 57 (1993) 179-182; [https://doi.org/10.1016/0257-8972\(93\)90037-0](https://doi.org/10.1016/0257-8972(93)90037-0)
- [3] F. Sanchette, C. Ducros, A. Billard, C. Rébéré, C. Berziou, M. Reffass, J. Creus, Nanostructured aluminium based coatings deposited by electron-beam evaporative PVD, *Thin Solid Films* 518 (2009) 1575–1580; doi:10.1016/j.tsf.2009.09.057
- [4] J. Creus, H. Idrissi, H. Mazille, F. Sanchette, P. Jacquot, Corrosion behaviour of Al Ti coating elaborated by cathodic arc PVD process onto mild steel substrate, *Thin Solid Films* 346 (1999) 150-154.
- [5] F. Sanchette, A. Billard, Main features of magnetron sputtered aluminium transition metal alloy coatings, *Surface and Coatings Technology* 142 (2001) 218-224; doi:10.1016/S0257-8972(01)01197-5
- [6] K. E. Knipling, D. C. Dunand, D. N. Seidman, Criteria for developing castable, creep resistant aluminium-based alloys – a review. *Z Metall.* 97 (2006) 246–265; doi:10.3139/146.101249
- [7] K. E. Knipling, D. C. Dunand, D. N. Seidman, Nucleation and precipitation strengthening in dilute Al–Ti and Al–Zr alloys, *Metall. Mater. Trans. A* 38 (2007) 2522–2563. doi:10.1007/s11661-007-9283-6.
- [8] P. H. Lamarão Souza, C. A. Silva de Oliveira, J. M. do Vale Quaresma, Precipitation hardening in dilute Al-Zr alloys, *J. Mater. Res. Technol.* 7 (2018) 66-72; doi:10.1016/j.jmrt.2017.05.006

- [9] D. Tsivoulas, J.D. Robson, Heterogeneous Zr solute segregation and Al<sub>3</sub>Zr dispersoid distributions in Al–Cu–Li alloys, *Acta Materialia* 93 (2015) 73–86; <http://dx.doi.org/10.1016/j.actamat.2015.03.057>
- [10] H. Liu, V.H. Nguyen, H. Roussel, I. Gélard, L. Rapenne, J.-L. Deschamps, C. Jiménez, D. Muñoz-Rojas, Cu<sub>2</sub>O thin films: The role of humidity in tuning the texture and electrical properties of Cu<sub>2</sub>O thin films deposited via aerosol-assisted CVD, *Adv. Mater. Interfaces* 6 (2019) 1970020. <https://doi.org/10.1002/admi.201970020>
- [11] JCPDS file n° 01-077-6861
- [12] JCPDS file n° 00-048-1385
- [13] C. Amador, J. J. Hoyt, B. C. Chakoumakos, D. de Fontaine, Theoretical and experimental study of relaxation in Al<sub>3</sub>Ti and Al<sub>3</sub>Zr ordered phases, *Phys. Rev. Lett.* 74 (1995) 4955.
- [14] Chaomin Zhang, Yong Jiang, Fuhua Cao, Tao Hu, Yiren Wang, Dengfeng Yin, Formation of coherent, core-shelled nano-particles in dilute Al–Sc–Zr alloys from the first-principles, *Journal of Materials Science Technology* 35 (2019) 930–938; <https://doi.org/10.1016/j.jmst.2018.11.004>
- [15] N. Ryum, Precipitation and recrystallization in an Al–0.5 wt.% Zr alloy, *Acta Metall.* 17 (1969) 269.
- [16] K. S. Vecchio, D. B. Williams, Convergent beam electron diffraction study of Al<sub>3</sub>Zr in Al–Zr and Al–Li–Zr alloys, *Acta Metall.* 35 (1987) 2959.
- [17] E. Clouet, Séparation de Phase dans les Alliages Al–Zr–Sc: du Saut des Atomes à la Croissance de Précipités Ordonnés, PhD thesis, Ecole Centrale des Arts et Manufactures, École Centrale Paris, 2004.
- [18] V. C. Gudla, K. Rechendorff, Z. I. Balogh, T. Kasama, R. Ambat, In-situ TEM investigation of microstructural evolution in magnetron sputtered Al–Zr and Al–Zr–Si coatings during heat treatment, *Materials and Design* 89 (2016) 1071–1078; <http://dx.doi.org/10.1016/j.matdes.2015.10.081>

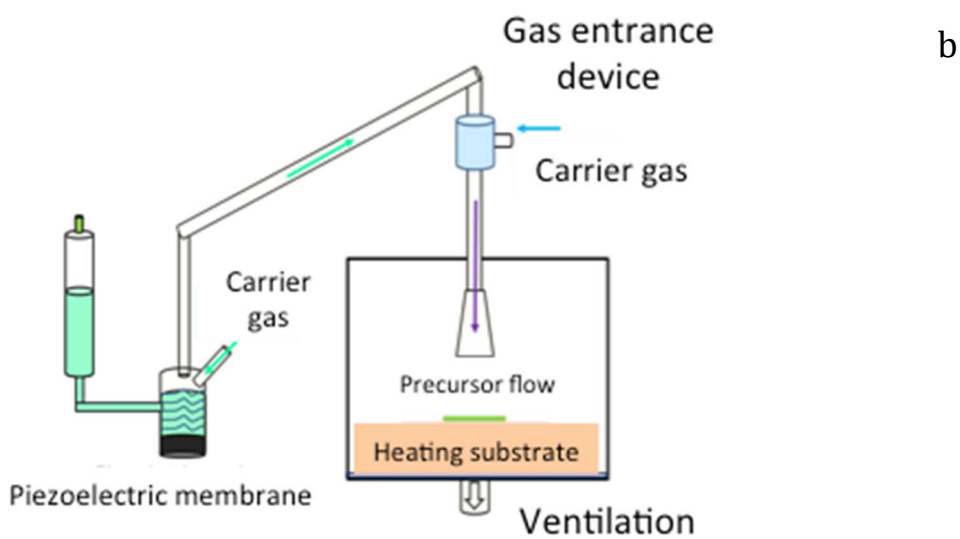
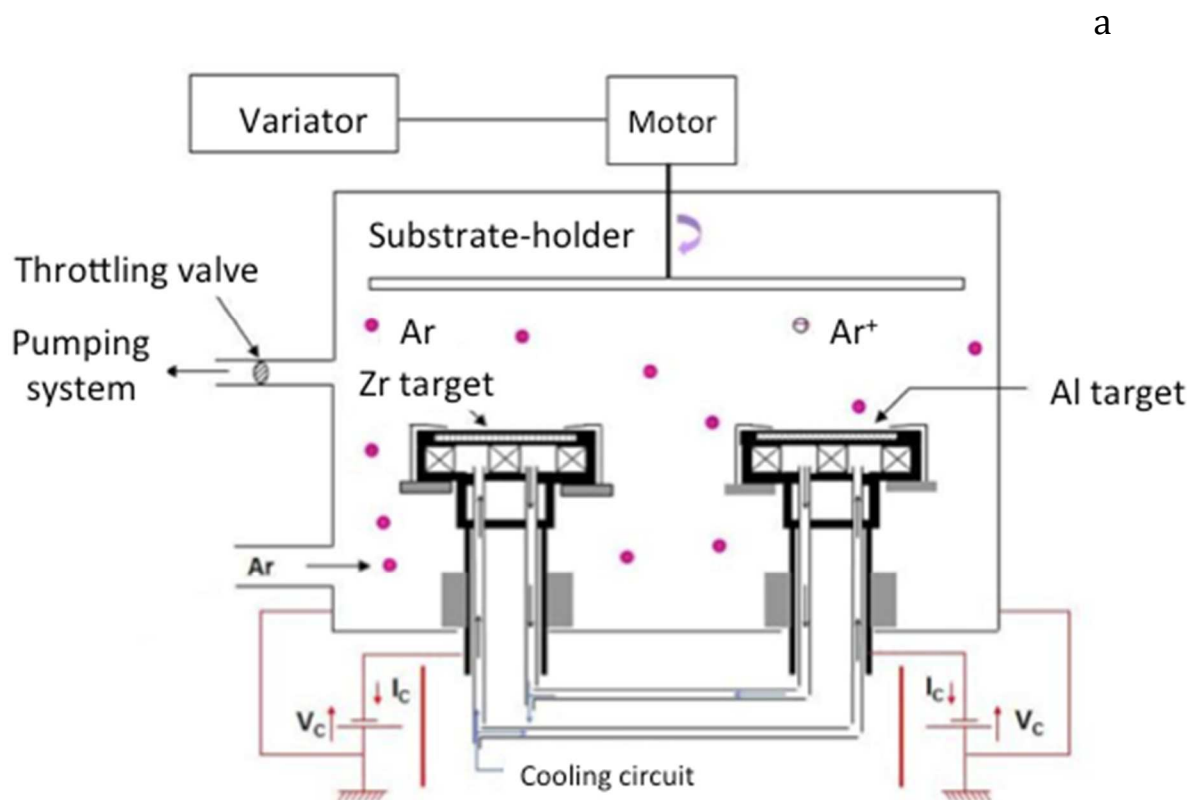


Fig. 1. Schemas of (a) the co-sputtering chamber and (b) Aerosol-Assisted Metal-Organic Chemical Vapour Deposition (AA-MOCVD) principle.

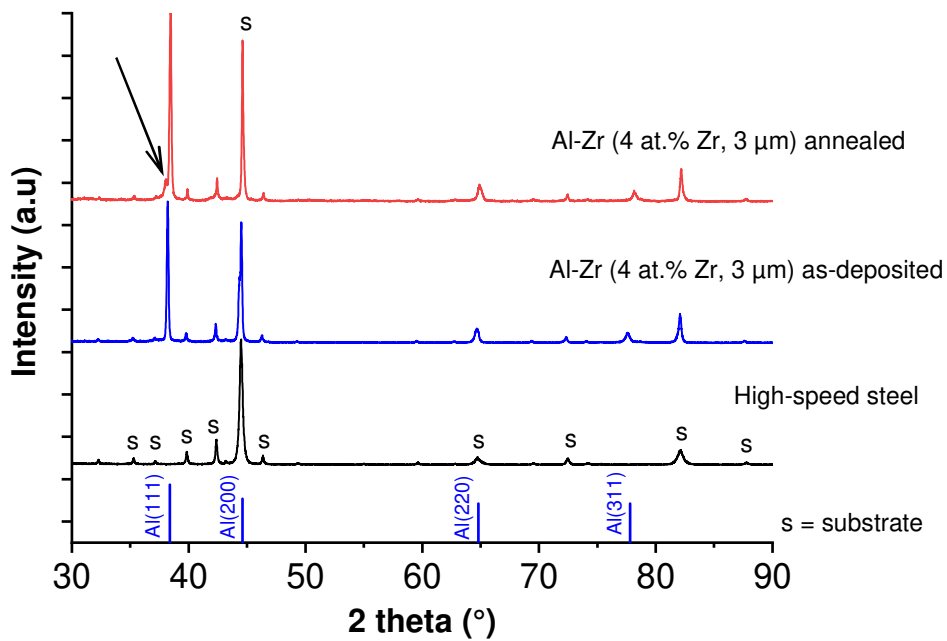


Fig. 2. XRD patterns of Al-Zr film deposited on high-speed steel substrate before and after annealing at 500 °C in air. From [1].

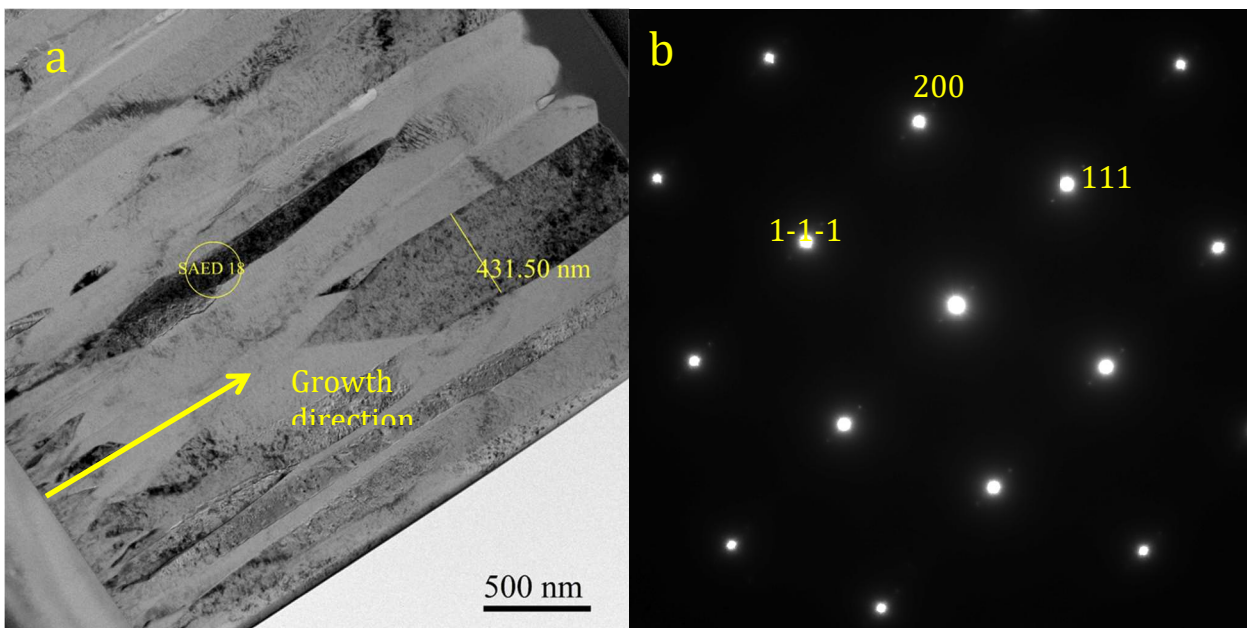


Fig. 3. Bright field TEM Image (a) and SAED pattern (b, [110] zone axis) of Al-Zr layer deposited before AA-MOCVD process (before annealing).

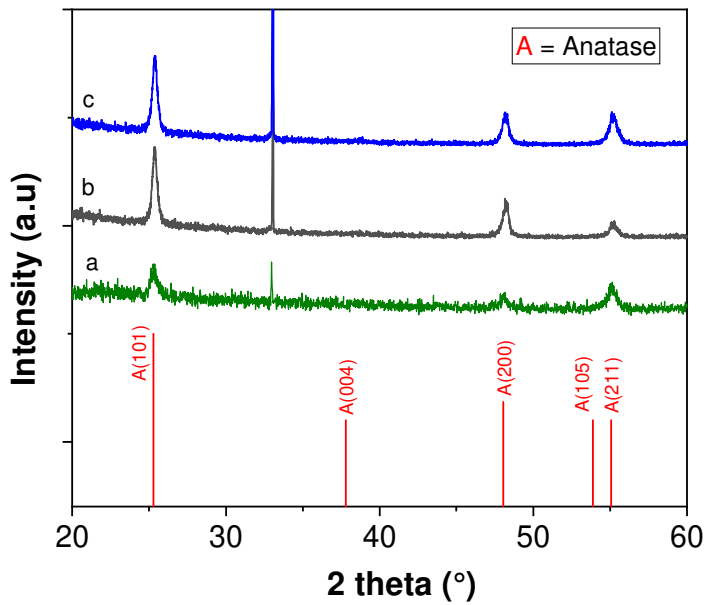


Fig. 4 XRD patterns of  $\text{TiO}_2$  films deposited on silicon substrate at a) 400 °C, b) 500 °C and c) 550 °C.

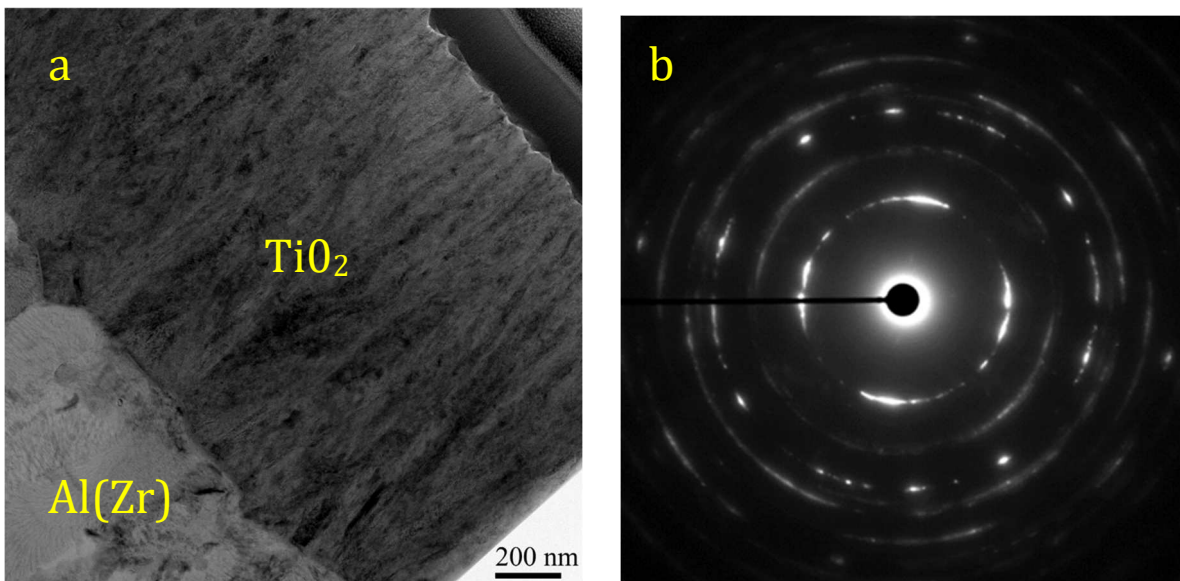


Fig. 5. Bright field TEM image (a) and SAED pattern (b, anatase  $\text{TiO}_2$ ) of  $\text{TiO}_2$  layer deposited on the Al-Zr coating.

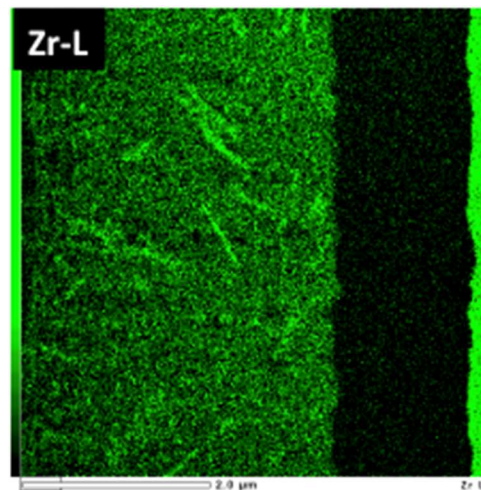
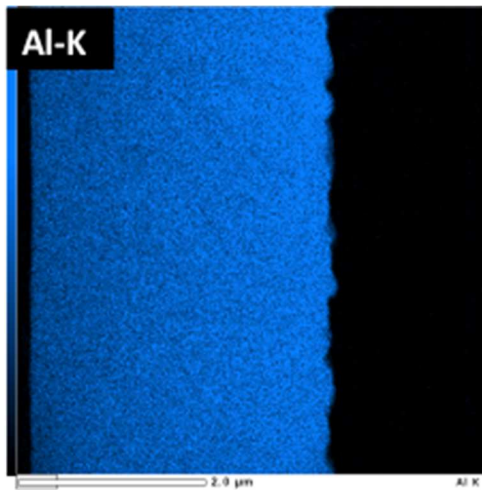
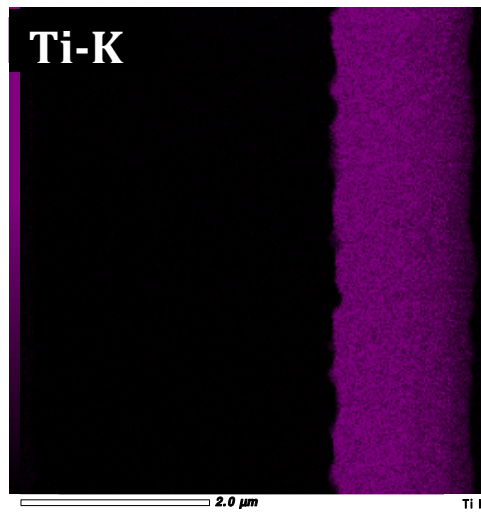
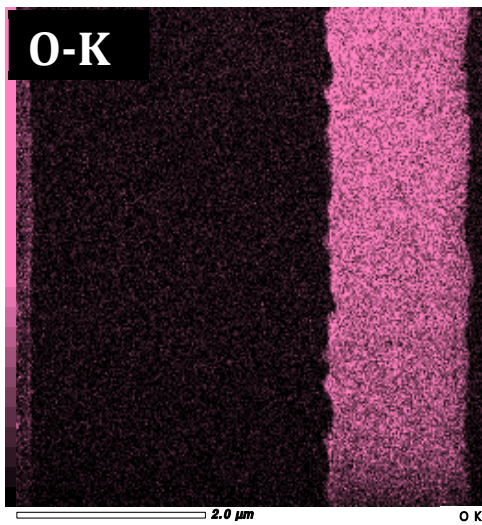
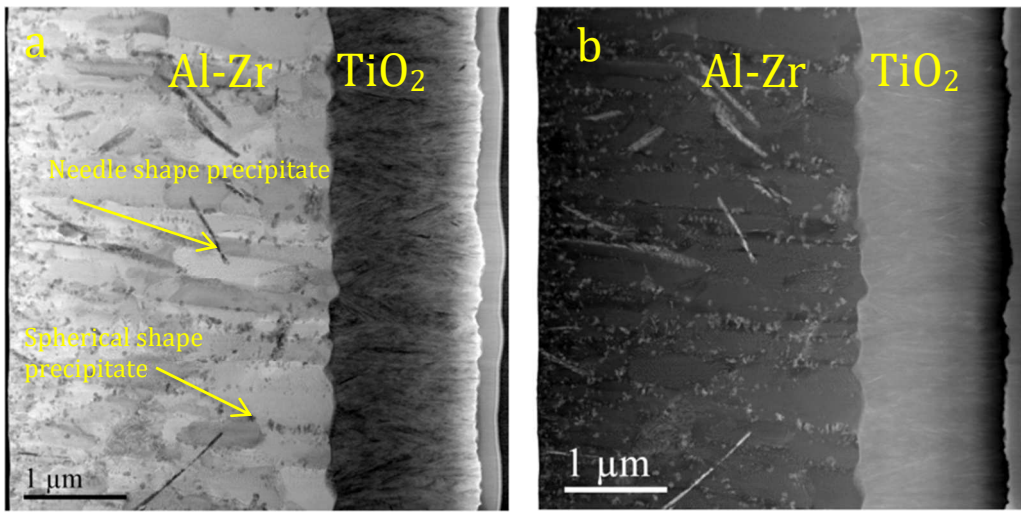


Fig. 6. STEM bright field (a) ; STEM HAADF (b) images and associated EDS elemental distribution maps of Al-Zr / TiO<sub>2</sub> bilayer. Precipitates richer in zirconium than the matrix have clearly two morphologies; needle and spherical.

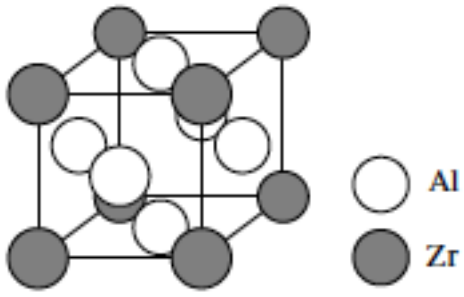


Fig. 7 Unit cell of L1<sub>2</sub> type for Al<sub>3</sub>Zr.

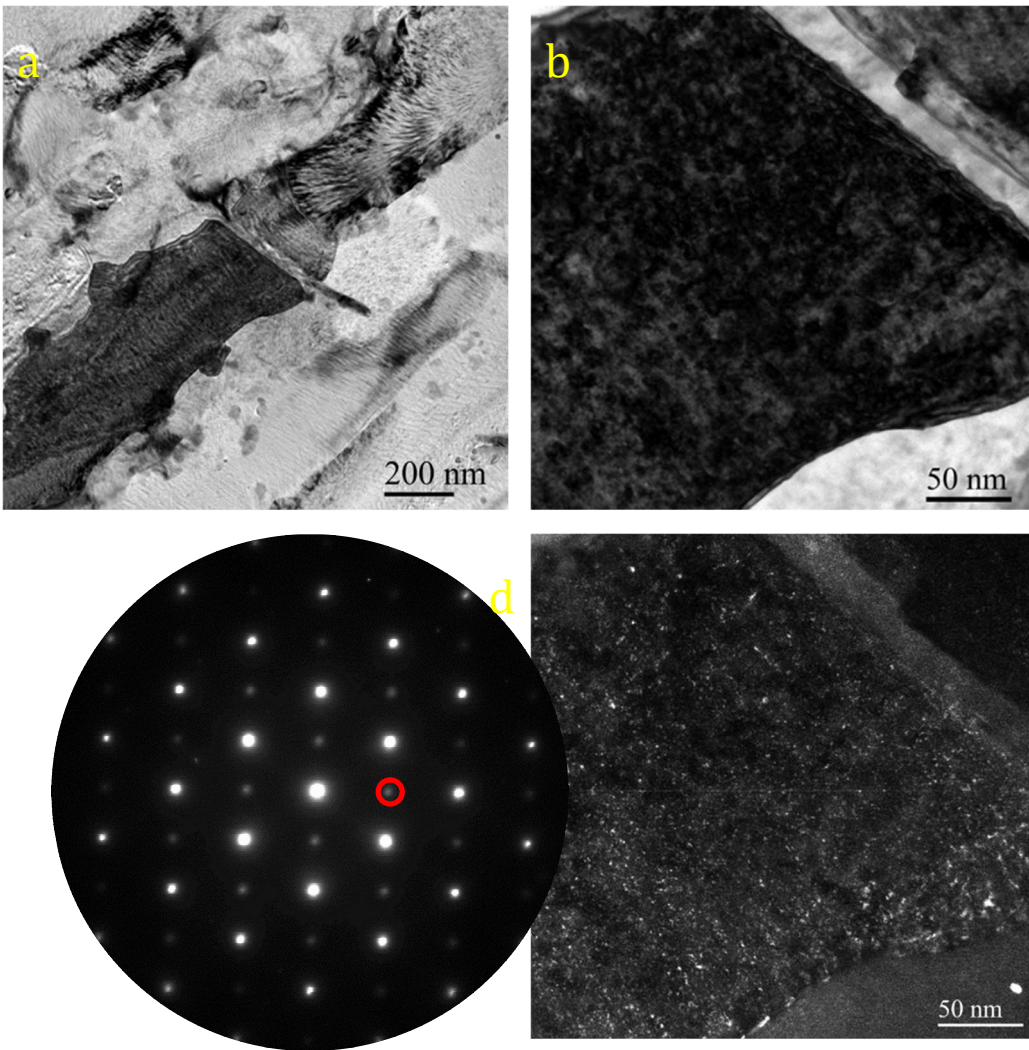


Fig. 8 Bright field (a, b zoomed) images, associated SAED pattern with the [110] zone axis (c) and dark field image (d) obtained from Al<sub>3</sub>Zr precipitates (red ring).

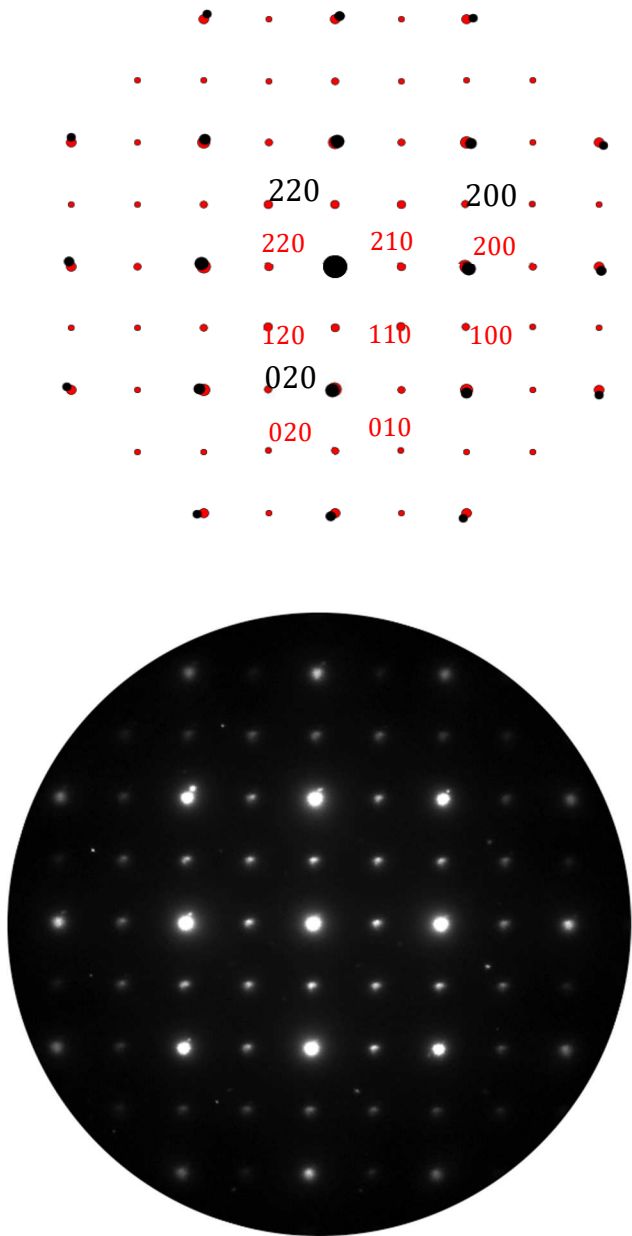


Fig. 9 Modelled (red:  $\text{Al}_3\text{Zr}(\text{L}1_2)$  and black :  $\text{Al}(\text{Zr})$ ) and SAED pattern of Al-Zr after AA-MOCVD process for  $\text{TiO}_2$  deposition (after annealing  $500^\circ\text{C}$ , 40 min).  $[\text{001}]\text{Al}_3\text{Zr}/[\text{001}]\text{Al}(\text{Zr})$ .

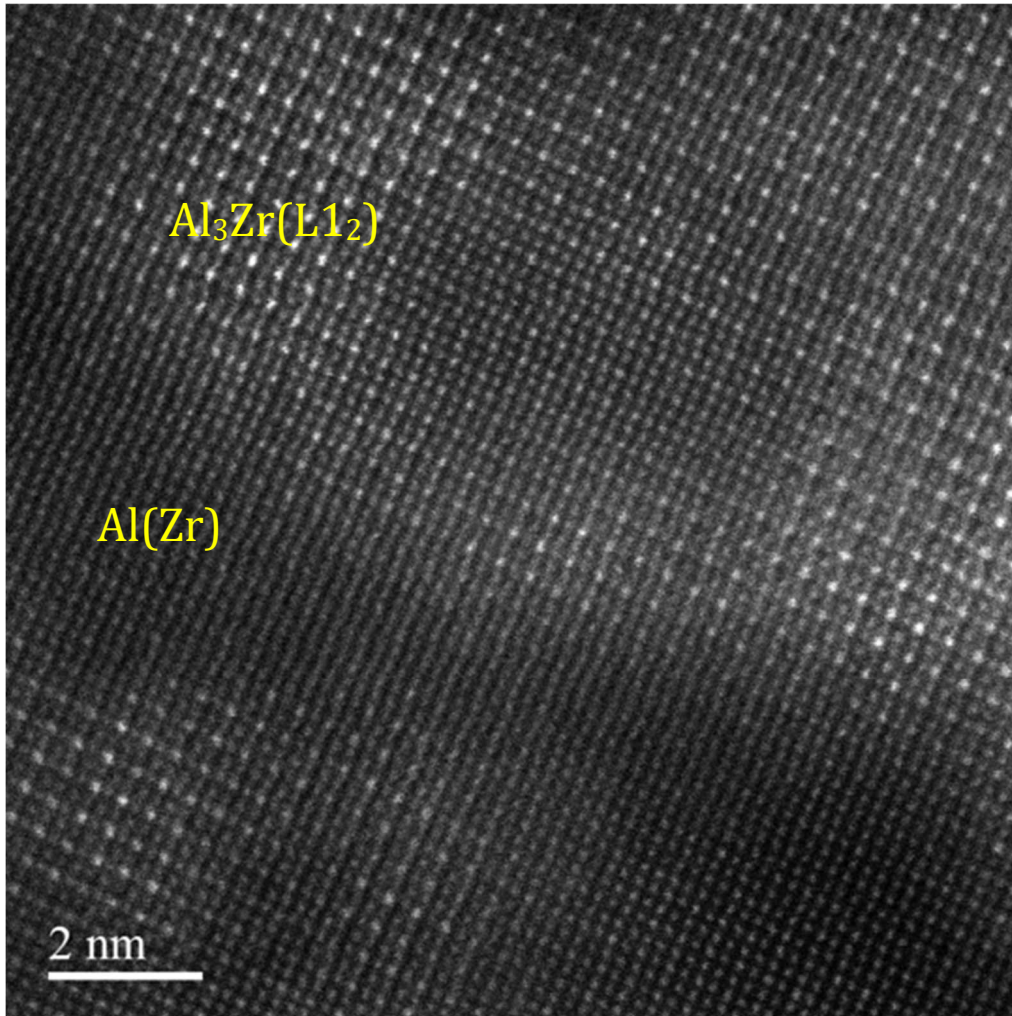


Fig. 10 High resolution STEM-HAADF **image** of Al-Zr coating after AA-MOCVD process for TiO<sub>2</sub> deposition (after annealing 500°C, 40 min).

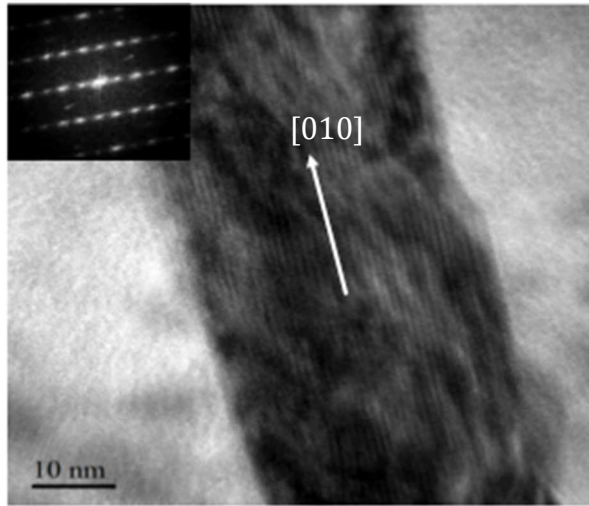


Fig. 11 HRTEM **image** and corresponding FFT ([100] zone axis). Needle-shape precipitates have the stable  $\text{Al}_3\text{Zr}(\text{DO}_{23})$  tetragonal structure.